Polymer Testing 125 (2023) 108137

Contents lists available at ScienceDirect

Polymer Testing

journal homepage: www.elsevier.com/locate/polytest

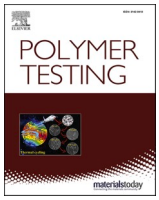

Experimental characterisation of the dilation angle of polymers

Gustavo Quino [a,b,*], Joseph Gargiuli [b], Soraia Pimenta [c], Ian Hamerton [b], Paul Robinson [a], Richard S. Trask [b]

[a] Department of Aeronautics, Imperial College London, SW7 2AZ, UK
[b] Bristol Composites Institute, University of Bristol, Queen's Building, University Walk, Bristol, BS8 1TR, UK
[c] Department of Mechanical Engineering, Imperial College London, SW7 2AZ, UK

ARTICLE INFO

Keywords:
Polymer
Plasticity
Dilation
Compression
Test method

ABSTRACT

Despite the wide use of Drucker-Prager plasticity-based models on polymers, the experimental measurement of the dilation angle, a critical parameter to fully describe the plastic potential, has been rarely reported in existing literature. This paper shows, for the first time, the experimental characterisation of the dilation angle of polymers over a wide range of plastic strain. These measurements were obtained from uniaxial compression experiments conducted on poly(methyl methacrylate) (PMMA) and an untoughened epoxy resin. The calculation of the dilation angle relied on the measurements of the compressive force and the strain components obtained *via* Digital Image Correlation (DIC). Lower values of dilation angle were obtained for the epoxy resin, suggesting that resistance to volumetric change during plastic deformation could be associated to molecular structure and internal forces. The methodology and results presented in this study can be applied to different types of materials and employed for developing and validating constitutive models that incorporate plastic dilation.

1. Introduction

Polymers are widely used in a variety of applications due to their excellent mechanical properties, lightweight, and relatively low cost. To design and analyse polymer-based structures or materials (*e.g.*, solid polymers, foams, polymer-based composites, *etc.*), it can be important to capture their behaviour accurately under different loading regimes. One of the challenges in modelling the behaviour of polymers is their complex and nonlinear response arising from their plastic, viscoelastic, and time-dependent nature.

Among the different constitutive models capable to reproduce the plastic behaviour of polymers, Drucker-Prager plasticity-based models are widely used due to their flexibility and ease of implementation [1–4]. One of the parameters required to fully define the plastic potential function and the flow rule in these models is the dilation angle ψ. Physically, the dilation angle correlates with the volume change during plastic deformation, commonly observed in polymers [5,6]. A higher dilation angle indicates higher dilatation or volume increase during plastic flow. In some cases, due to the lack of experimental data or for simplicity, the dilation angle ψ is considered equal to the friction angle β (associated flow rule) [1,7,8]. However, this assumption overlooks the actual volumetric dilation that may occur during plastic flow. To accurately describe plastic dilation, a non-associated flow rule may be necessary, requiring the measurement of the dilation angle parameter.

To the knowledge of the authors, the literature reporting the characterisation of the dilation angle of polymers is limited. Some authors reported on the plastic Poisson's ratio, directly related to the dilation angle as will be shown in Section 2.3. Dean and Crocker measured the plastic Poisson's ratio of a toughened epoxy adhesive from tensile experiments, combining strain measurements obtained *via* contact extensometers and strains indirectly measured using analytical corrections for machine's compliance [9]. However, owing to practical limitations of the extensometers, large strains could not be achieved. In addition, tensile experiments and contact extensometers do not provide valid results whenever strain localisation such as necking occurs. Morelle et al. reported on the plastic Poisson's ratio of the commercial epoxy resin RTM6, based on a highly cross-linked tetra-epoxide, obtained from axial and transverse measurements of strains with a linear variable differential transformer (LVDT) and analysis of images taken during the experiments [10]. No further details on the image analysis were provided, and the plastic Poisson's ratio was only reported for a plastic strain of 3%.

In this paper, we propose a methodology to measure the dilation angle of polymers over a large range of strains using non-contact full

* Corresponding author. Department of Aeronautics, Imperial College London, SW7 2AZ, UK.
E-mail address: g.quino-quispe@imperial.ac.uk (G. Quino).

https://doi.org/10.1016/j.polymertesting.2023.108137
Received 26 May 2023; Received in revised form 28 June 2023; Accepted 30 June 2023
Available online 1 July 2023

field strain measurements obtained *via* Digital Image Correlation (DIC). A thermoset and a thermoplastic polymer were selected to demonstrate the measurement protocol. The aim is to generate a procedure to measure the dilation angle of polymers, with the possible application to other materials. This methodology will improve the accuracy and reliability of constitutive models with non-associated flow rules. The results of this study will also contribute to a better understanding of the plastic deformation behaviour of polymers and improve the design and analysis of polymer-based structures and products. The accurate measurement of this parameter can be particularly relevant in micromechanical modelling of composites which has recently gained popularity in the composites community [1,8,11–13]. The matrix, confined between the fibres or other reinforcements, dilates and develops hydrostatic stresses under external loads which due to their pressure sensitivity, is relevant to calculate the different responses, especially when non-linearity and plastic deformation occur.

The following section provides a detailed description of the materials, specimen design, experimental methods, and data reduction procedures used in this study. The results obtained for the two materials are then presented and discussed in Section 3. A sensitivity analysis was conducted to evaluate the potential impact of errors in the measurements of the elastic properties. The concluding remarks, implications and future research directions are summarised in the final section.

2. Experimental

2.1. Materials and specimens

Two materials, a thermoplastic and a thermoset, were considered in this study. Poly(methyl methacrylate) (PMMA) was purchased in the form of a 15 mm thick commercial plate. A proprietary untoughened epoxy resin (*ex* Solvay, $T_g = 200°C$) was cast into cylindrical rods of 12.7 mm diameter, following the curing cycle recommended by the manufacturer (2 h @ 180°*C*).

All compression specimens were machined to cylinders of 6 mm diameter and 6 mm height as per the geometry shown in Fig. 1. This 1:1 aspect ratio geometry was found to display less barrelling in comparison to longer aspect ratios [14,15], improving the stress uniaxiality of the experiments at large deformations. To have statistically representative results, at least five specimens of each material were tested. The cylindrical surfaces of the coupons were prepared with a fine airbrush generated black speckle on white paint to conduct DIC.

2.2. Mechanical characterisation

The experimental setup is shown in Fig. 2. Quasi-static tests were conducted in the servo-hydraulic universal testing machine Instron 8872 (Instron, USA). Compression platens of 30 mm diameter and mirror surface finish were especially designed to fit the machine and to uniformly transmit the compressive load onto the specimens. The experiments were conducted in quasi-static regime under displacement control, at a prescribed constant crosshead speed of 0.006 mm/s, corresponding to a nominal strain rate of 0.001/s. Tests were manually stopped after a strain of at least 0.6 was reached. To minimise the effects of friction, Teflon tape 3 M 5480 (3 M, USA) was placed between the loading platens and the flat ends of the specimen as in Ref. [15]. The use of Teflon tape showed a higher reduction of barrelling than other lubricants.

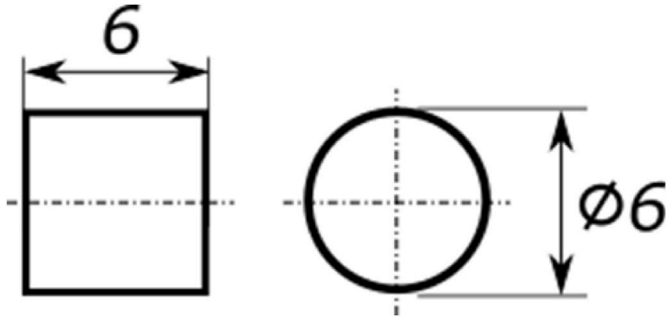

Fig. 1. Dimensions of the compression specimens (mm).

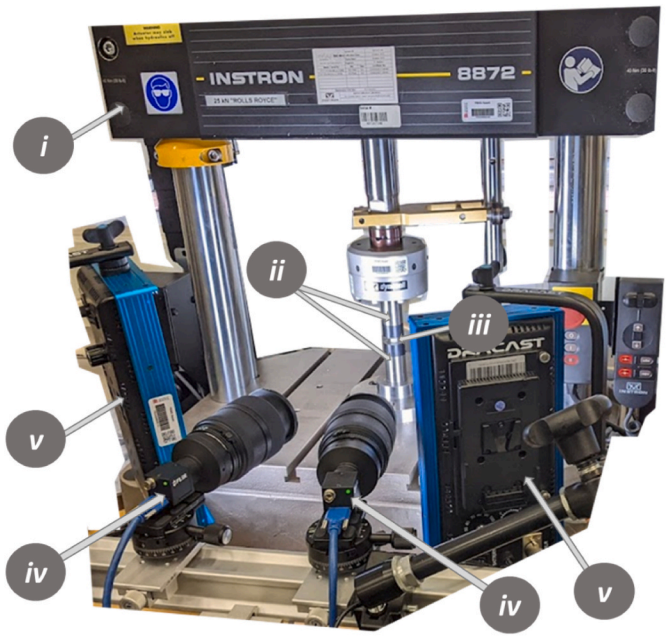

Fig. 2. Experimental setup: i) Testing machine, ii) Loading platens, iii) Specimen, iv) USB3 Cameras, and v) LED lights.

The load histories were obtained from the Instron 25 kN (Instron, USA) load cell mounted in the testing apparatus. During the experiments, images of the speckled specimens were acquired with two USB3 cameras Flir S BFS–U3–123S6M − C (Teledyne Flir, USA) at a rate of 1 image per second with 12.3 MP resolution. Artificial illumination was provided by two LED lights conveniently set to improve contrast and depth of field in the images. The average speckle size was approximately 4.8 pixels. To assess the quality of the speckle pattern, the mean intensity gradient was measured as in Refs. [16,17] and found to be 21.2 which corresponds to a good quality of speckle pattern. The series of images were postprocessed using stereo digital image correlation (subset size 31 pixels, step size 10 pixels) with the software DaVis 10 (LaVision, Germany).

2.3. Data reduction

Strains and stresses reported and discussed in this manuscript are true (i.e., logarithmic) strains and true stresses. The strains were obtained *via* DIC analysis. A representative virtual strain gauge (VSG) located in the centre of the specimen, of approximately 70 × 70 pixels size (0.37 mm × 0.37 mm), was used to extract the strain components. The true stress σ_t^z was calculated by dividing the (negative) load F by the true cross-sectional area:

$$\sigma_t^z = \frac{F}{A_o e^{2\varepsilon_t^r}} \tag{1}$$

Where A_o is the initial cross-sectional area, and ε_t^r is the radial true strain.

The elastic modulus E was measured from the initial linear part of the axial strain ε_t^z *vs.* stress σ_t^z curves, *via* a linear regression within the axial strain range $0 < \varepsilon_t^z < 0.015$, within the linear response. The Poisson's ratio ν was obtained from a linear regression of the radial and axial

strains ε_t^r and ε_t^z, also within the axial strain range $0 < \varepsilon_t^z < 0.015$.

To calculate the dilation angle, the entire histories of strains and axial stresses are required. The analysis starts with the decomposition of the total true strain ε_t into elastic ε_e and plastic ε_p components using the additive decomposition:

$$\varepsilon_t = \varepsilon_e + \varepsilon_p \tag{2}$$

Defining a cylindrical coordinate system with axis coincident with the specimen's axis, the axial and radial true strain components, ε_t^z and ε_t^r respectively, can also be decomposed into their elastic and plastic parts as shown in Eqs. (3) and (4).

$$\varepsilon_t^z = \varepsilon_e^z + \varepsilon_p^z \tag{3}$$

$$\varepsilon_t^r = \varepsilon_e^r + \varepsilon_p^r \tag{4}$$

The true axial strain ε_t^z and true hoop strain ε_t^θ can directly be obtained from the DIC analysis of the cylindrical surface. The radial component ε_t^r, under the assumption of axisymmetric deformation, is always equal to the hoop strain ε_t^θ. An analytical proof and an experimental validation of this statement can be found in Appendix A.

For an isotropic material under uniaxial true compressive stress σ_t^z, using Eqs. (3) and (4), the plastic axial and radial components of the strain, ε_p^z and ε_p^r respectively, can be calculated as:

$$\varepsilon_p^z = \varepsilon_t^z - \frac{\sigma_t^z}{E} \tag{5}$$

$$\varepsilon_p^r = \varepsilon_t^r + \nu\frac{\sigma_t^z}{E} \tag{6}$$

where E and ν are the elastic modulus and Poisson's ratio of the polymer, respectively.

The plastic Poisson's ratio ν_p, under uniaxial load, is defined as the negative ratio between the transverse and the axial plastic strain:

$$\nu_p = -\frac{\varepsilon_p^r}{\varepsilon_p^z} \tag{6a}$$

Finally, the dilation angle ψ can be evaluated as a function of the plastic Poisson's ratio ν_p using Eq. (7), as in Refs. [9,10,18]:

$$\psi = \tan^{-1}\left(-\frac{3(1-2\nu_p)}{2(1+\nu_p)}\right) \tag{7}$$

The equations above show that the dilation angle ψ, under uniaxial loading, only depends on the plastic Poisson's ratio. This parameter can be obtained from the history of load σ_t^z, the history of strain components ε_t^z, ε_t^r; and the elastic material constants E, and ν, as shown in Eqs. (4)–(6).

3. Results and discussion

3.1. Compressive behaviour

Fig. 3 shows the DIC full field measurements of axial strain ε_t^z for one representative specimen of each material, at different levels of compressive strain. The fact that the lateral edges of the specimens remained nearly parallel during the test confirms that use of Teflon tape prevented significant barrelling effects in the experiments. Fig. 3 also shows the uniformity of the strain field, suggesting that the whole volume of the specimen mainly stayed under uniaxial loading conditions during the test, even up to large deformations. The uniformity observed in the strain maps also validates the assumption of axisymmetric deformation, required for the data reduction procedure described in Section 2.3.

Fig. 4a and b shows the true stress *vs.* true strain curves for PMMA

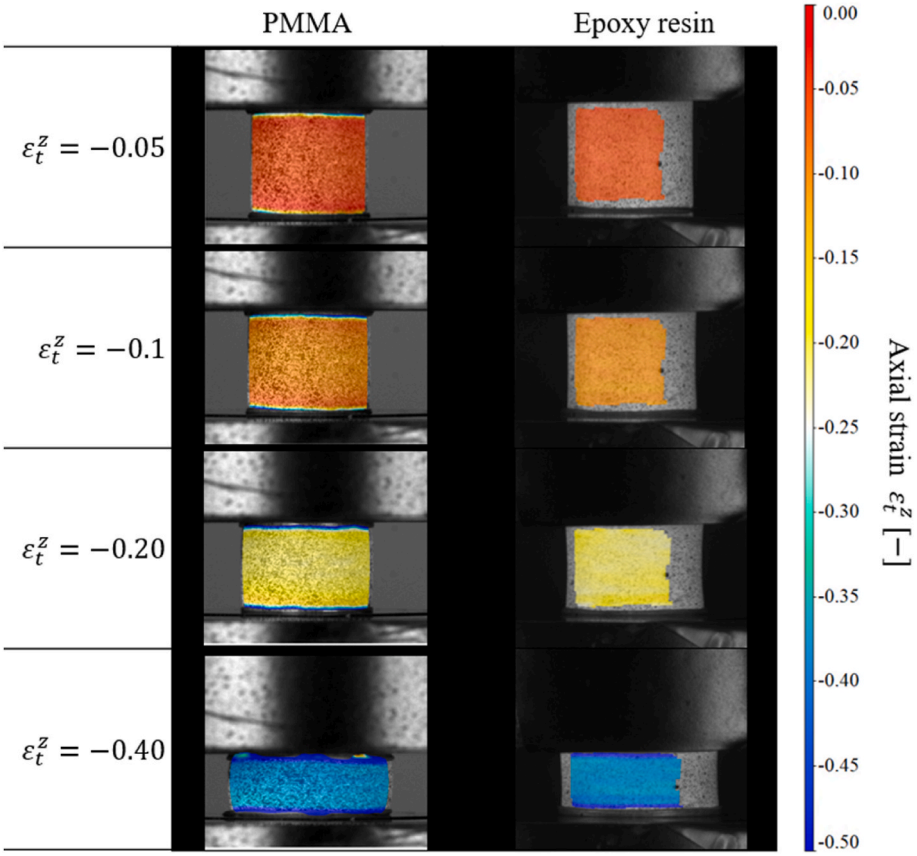

Fig. 3. Full field measurements of axial strain ε_t^z obtained from DIC.

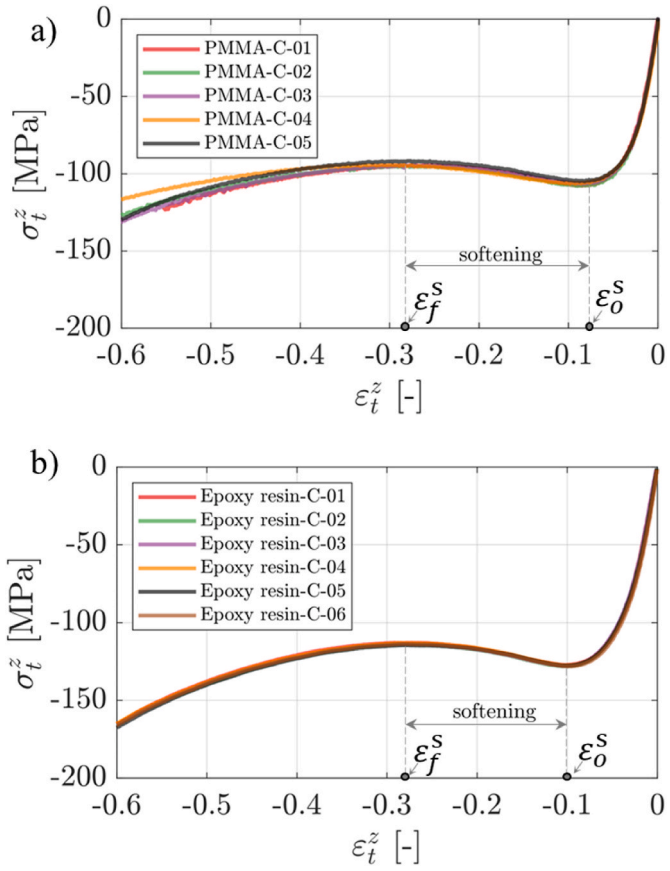

Fig. 4. Axial true stress σ_t^z *vs.* true strain ε_t^z curves for a) PMMA and b) untoughened epoxy resin.

and epoxy resin respectively. Both strains and stresses are compressive and therefore represented by negative values; for PMMA and epoxy resin, the initial part of the plot is linear. With increasing axial strain, the material yields with a progressive reduction of the tangent modulus, followed by a local maximum stress. After this local maximum stress, at strain ε_o^s, the softening regime starts, with a continuous decrease of the compressive stress until strain ε_f^s, possibly driven by the restructuring of molecular chains [19]. The next regime in the strain *vs.* stress curve is the strain hardening, where compressive stress increases with strain, mainly driven by the resistance to chain alignment [20–22]. This type of behaviour has been previously reported for various types of polymers in the literature [19,23]. The untoughened epoxy resin exhibits similar overall behaviour, but yields, softens, and hardens at higher stresses (Fig. 4b). None of the specimens fractured in the experiments.

The average measurements and standard deviations of elastic moduli, Poisson's ratio, and softening strains are summarised in Table 1. The average measured PMMA's elastic modulus of 3.20 GPa is consistent with previously reported values [21]. The measured Poisson's ration of PMMA was 0.45. The elastic modulus obtained for the epoxy resin of 3.24 GPa, and the Poisson's ratio of the epoxy resin of $\nu = 0.43$ fall within the ranges previously reported for other epoxy resin systems [24].

Table 1
Elastic material constants and softening strains evaluated from the experiments.

Material	E [GPa]	ν [−]	ε_o^s [−]	ε_f^s [−]
PMMA	3.20 ± 0.11	0.45 ± 0.03	0.084 ± 0.003	0.282 ± 0.001
Epoxy resin	3.24 ± 0.07	0.43 ± 0.01	0.100 ± 0.002	0.275 ± 0.004

3.2. Dilation angle

From Eqs. (1)–(5) and the elastic parameters from Table 1, the plastic components of the strain were calculated. Representative sets of radial and axial components of plastic strain *vs.* total axial strain obtained from PMMA and epoxy resin samples are shown in Fig. 5a and b respectively. Initially, both plastic axial and radial components are zero during the linear regime, where there is no plasticity. After an initial non-linear region, both components follow an almost linear trend with respect to the total axial strain, approximately starting from the beginning of the softening regime; a similar trend was also observed in the epoxy resin.

Since the dilation angle is only defined when there is plasticity, we present it as a function of the plastic strain. The dilation angles *vs.* plastic axial strain ε_p^z, for PMMA and epoxy resin, are shown in Fig. 6a and b respectively. The dilation angle of PMMA displays a decreasing trend at small plastic strains. The values of the dilation angle of PMMA stabilise after a plastic strain of approximately 0.15, after which is becomes linear with respect to the axial strain. Fig. 6b shows that the dilation angle of the epoxy resin with respect to the plastic axial strain. It also exhibits a decreasing trend at low plastic strains. In this case, stabilisation occurs after a plastic strain of approximately 0.2, after which the dilation angle becomes linear with the plastic strain. Since the dilation angle does not show a stable value at small plastic strains or even within part of the softening region, a representative value of this parameter should better be measured after full softening has taken place.

Even after the dilation angle becomes stable, there seems to be a consistent increase with axial strain. To the authors' knowledge, most Drucker-Prager plasticity models currently implemented in commercial FE software cannot account for a variable dilation angle or even negative as was observed in the epoxy resin. The slope within of the dilation angle within the stable region has a magnitude of 6.7° per unit of strain in the case of the PMMA, and 9.4° per unit of strain for epoxy resin, measured from the slopes of the dilation angle within the stable region. For the purposes of comparison, we select a representative value of the dilation angle at plastic strain of 0.3.

The average dilation angle of the PMMA at a plastic strain of 0.3 was $7.84 \pm 1.31°$. This value is smaller than the friction angle $\beta = 20°$ found by Rueda-Ruiz et al. via inverse modelling [25]. This mismatch agrees with previously reported findings showing that associated flow rules ($\psi = \beta$) overestimate the plastic dilatancy of polymers [26]. Therefore, a non-associative flow rule should be used to model the plastic behaviour of PMMA.

The average dilation angle of the untoughened epoxy resin at a plastic strain of 0.3 was $-1.50 \pm 0.52°$. In Refs. [9,10], respectively, the plastic Poisson's ratios for an epoxy adhesive (measured in tension) and RTM6 epoxy resin (measured in compression) were reported. The corresponding dilation angles were 28.51 ° and 0 ° respectively. In another study, Sorini et al. [27] calibrated their constitutive model accounting for tension/compression asymmetry in RTM6. They found different values of dilation angle under tension and compression, 14.28 ° and −0.001 °, respectively. Comparison of our measurements with those described above show that the dilation angle of thermoset epoxy resins is close to zero under compression. These low values of the compression dilation angles indicate that the plastic volumetric flow is close to isochoric.

The variation in plastic dilatancy between PMMA and epoxy resin may be related to differences in molecular structure and internal forces. From the structural perspective, the aliphatic nature of PMMA is expected to enable greater chain rotations compared to the epoxy resin, where the highly cross-linked network causes limited segmental motion [28,29]. The internal forces in these polymers are also different. The PMMA would predominantly have dipole-dipole interactions, while in the epoxy resin there are hydrogen bonds, stronger than the dipole-dipole forces [30]. Molecular dynamics simulations conducted by Peng et al. have suggested that polymers with longer chains, and

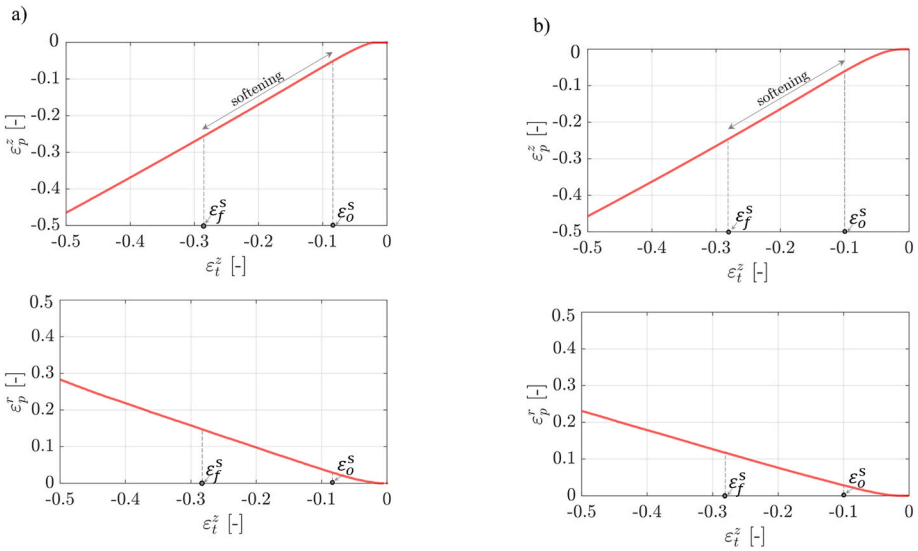

Fig. 5. Typical plastic strain components *vs.* axial strain extracted from a representative test on a) PMMA, and b) Epoxy resin.

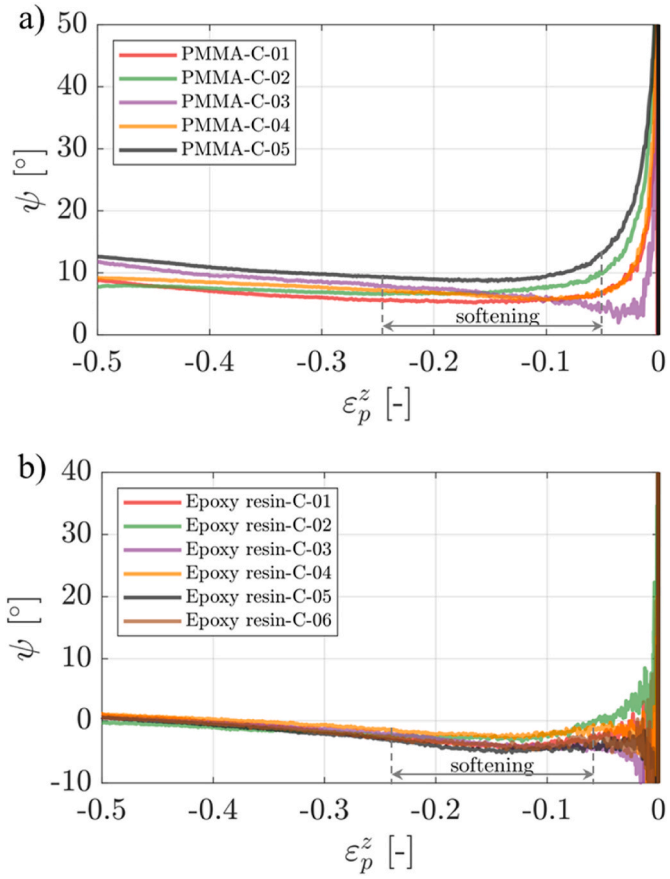

Fig. 6. Dilation angle ψ *vs.* plastic axial strain ε_p^z for a) PMMA and b) untoughened epoxy resin.

consequently higher internal forces, exhibit smaller volume dilation [31]. The highly cross-linked structure and the higher internal forces in the epoxy resin could therefore cause its limited segmental motion and higher resistance to volume change, leading to the observed reduced plastic dilation.

3.3. Sensitivity study

The evaluation of the dilation angle ψ depends on the elastic properties such as elastic modulus E and Poisson's ratio ν (Equations (1)–(7)) and could then be sensitive to errors in their characterisation. A parametric analysis was conducted to assess the sensitivity of the presented method to possible errors in the measured values of elastic parameters. A representative PMMA test was selected for this exercise. The analysis considered a parametric sweep of different values of Poisson's ratio, in steps of 0.04, and three values of elastic modulus in steps of 0.3 GPa with central values equal to the averaged experimental measurements.

Fig. 7 shows how the dilation angle is affected by these varying elastic parameters. Overall, lower values of elastic modulus and Poisson's ratio lead to higher dilation angles. The curves are mostly affected at smaller plastic strains. For the parametric sweep, the dilation angle shows a standard deviation of ±4.41° at a small plastic strain of 0.02. However, at a plastic strain of 0.3, the standard deviation reduces to ± 0.36 °. This smaller uncertainty also supports the earlier observation that a more representative value of the dilation angle can be obtained after the strain softening regime.

4. Conclusions

In this paper, uniaxial compression tests were conducted to experi-

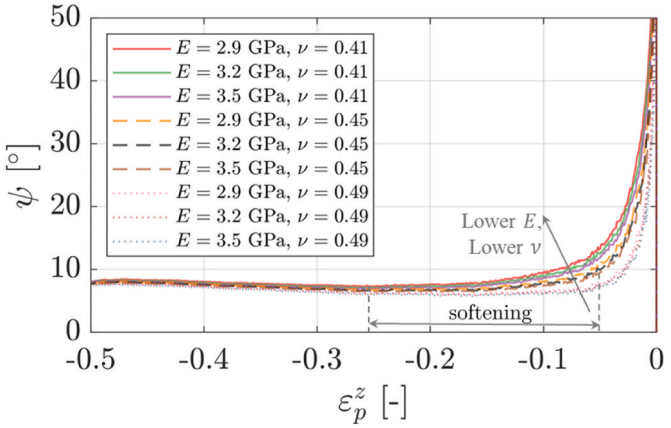

Fig. 7. Sensitivity analysis of the dilation angle with respect to the variability of elastic properties E and ν.

mentally measure the dilation angle ψ, a relevant parameter in Drucker-Prager plasticity models with non-associated flow, and directly linked to plastic dilatancy. One thermoset and one thermoplastic polymer were selected to demonstrate the proposed methodology. Digital image correlation was employed to obtain a full map of the strain components. A parametric study was also conducted to assess the influence of possible measurement errors in the method herein presented. The main conclusions are:

- The presented technique allows for the calculation of the dilation angle of polymers from uniaxial compression up to large strains.
- The dilation angle of PMMA is smaller than its friction angle. Therefore, it follows a non-associated flow rule.
- The untoughened epoxy resin displays a plastic flow nearly isochoric under compressive loads.
- The untoughened epoxy resin has a smaller angle of dilation than the PMMA, possibly due to its highly cross-linked polymeric network.
- While not perfectly constant as the axial strain increases, the dilation angle shows less variability after full material softening, where possible errors in the measured elastic modulus or Poisson's ratio have minimal influence.

The methodology herein presented will help to build more reliable and accurate constitutive models for polymers. Our future research activities include the incorporation of these experimental measurements in the development of high-fidelity micromechanical models for fibre composite materials. Some relevant questions that remain open include the tension-compression asymmetry, effects of temperature, strain rate upon plastic dilation.

CRediT author statement

Gustavo Quino: Conceptualization, Methodology, Validation, Formal analysis, Investigation, Writing- Original draft preparation, Writing - Review & Editing, Visualization. Joseph Gargiuli: Investigation, Writing - Review & Editing. Soraia Pimenta: Conceptualization, Methodology, Writing - Review & Editing, Supervision. Ian Hamerton: Resources, Writing - Review & Editing, Writing - Review & Editing, Supervision, Project administration. Paul Robinson: Conceptualization, Methodology, Writing - Review & Editing, Supervision. Richard S. Trask: Conceptualization, Methodology, Resources, Writing - Review & Editing, Supervision, Project administration, Funding acquisition.

Declaration of competing interest

The authors declare that they have no known competing financial interests or personal relationships that could have appeared to influence the work reported in this paper.

Data availability

Data will be made available on request.

Acknowledgements

Authors acknowledge the support of by UK Engineering and Physical Sciences Research Council (EPSRC) programme Grant EP/T011653/1, Next Generation Fibre-Reinforced Composites: a Full Scale Redesign for Compression, a collaboration between Imperial College London and the University of Bristol. We thank Solvay (Wrexham) for the provision of the untoughened epoxy resin and assistance with sample manufacturing and Dr Mark Harriman and Dr Jon Meegan for useful discussions. For the purpose of open access, the author has applied a Creative Commons Attribution (CC BY) licence to any Author Accepted Manuscript version arising.

Appendix A. Radial and hoop strain components

If the circular cross-sections remain circular during the compression tests, the radial component and the hoop component of the strain tensor measured on the surface of the cylindrical specimens must be the same.

Given an initial radius of the undeformed cross section r_1 that grows to r_2, the true hoop strain ε_t^θ is:

$$\varepsilon_t^\theta = \ln\left(\frac{2\pi r_2}{2\pi r_1}\right) \tag{A.1}$$

After simplification of the 2π term in both numerator and denominator, the hoop component is equal to the radial component as we initially intended to proof:

$$\varepsilon_t^\theta = \ln\left(\frac{r_2}{r_1}\right) = \varepsilon_t^r \tag{A.2}$$

The validity of this assumption was cross-checked against experimental measurements obtained with DIC (Fig. A.1), using the same processing settings described in Section 2.2. One virtual extensometer with start and end at opposite edges of the specimen was created to measure the radial strain ε_t^r . In addition, a virtual strain gauge of 70 × 70 pixels size, approximately 2.3 times the subset and 7 times the step size, was created in the middle of the extensometer to measure the hoop component of strain ε_t^θ. Fig. A.1 shows that these two sources provide with the same values during all the experiment.

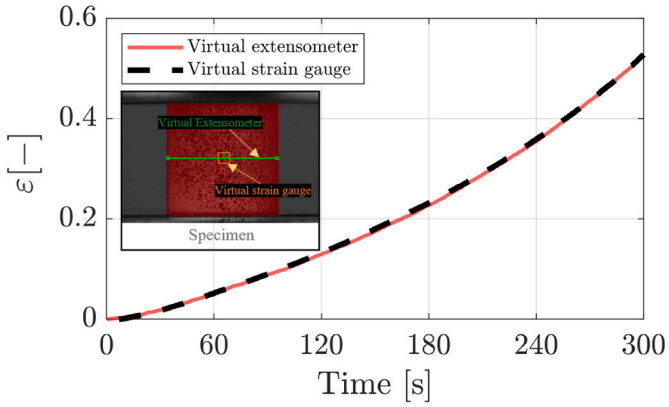

Fig. A.1. Histories of radial strain obtained from the virtual extensometer, and hoop strain measured from a virtual strain gauge at the centre of the specimen's surface.

References

[1] D. Pulungan, G. Lubineau, A. Yudhanto, R. Yaldiz, W. Schijve, Identifying design parameters controlling damage behaviors of continuous fiber-reinforced thermoplastic composites using micromechanics as a virtual testing tool, Int. J. Solid Struct. 117 (Jun. 2017) 177–190, https://doi.org/10.1016/j.ijsolstr.2017.03.026.

[2] F. Naya, C. González, C.S. Lopes, S. Van der Veen, F. Pons, Computational micromechanics of the transverse and shear behavior of unidirectional fiber reinforced polymers including environmental effects, Composer Part A Appl Sci Manuf 92 (Jan. 2017) 146–157, https://doi.org/10.1016/j.compositesa.2016.06.018.

[3] J. Chen, L. Wan, Y. Ismail, P. Hou, J. Ye, D. Yang, Micromechanical analysis of UD CFRP composite lamina under multiaxial loading with different loading paths, Compos. Struct. 269 (Aug. 2021), 114024, https://doi.org/10.1016/j.compstruct.2021.114024.

[4] D.C. Drucker, W. Prager, Soil mechanics and plastic analysis or limit design, Q. Appl. Math. 10 (2) (1952) 157–165. Feb. 21, 2023. [Online]. Available: https://www.jstor.org/stable/43633942.

[5] M. Kitagawa, T. Yoneyama, Plastic dilatation due to compression in polymer solids, J. Polym. Sci., Polym. Lett. Ed. 26 (4) (Apr. 1988) 207–212, https://doi.org/10.1002/pol.1988.140260407.

[6] B. Vorselaars, A.V. Lyulin, M.A.J. Michels, Deforming glassy polystyrene: influence of pressure, thermal history, and deformation mode on yielding and hardening, J. Chem. Phys. 130 (7) (Feb. 2009), 074905, https://doi.org/10.1063/1.3077859.

[7] M. Rueda-Ruiz, M. Herráez, F. Sket, F. Gálvez, C. González, J.M. Molina-Aldareguia, Study of the effect of strain rate on the in-plane shear and transverse compression response of a composite ply using computational micromechanics, Composer Part A Appl Sci Manuf 168 (May 2023), 107482, https://doi.org/10.1016/j.compositesa.2023.107482.

[8] F. Naya, C. González, C.S. Lopes, S. Van der Veen, F. Pons, Computational micromechanics of the transverse and shear behavior of unidirectional fiber reinforced polymers including environmental effects, Composer Part A Appl Sci Manuf 92 (Jan. 2017) 146–157, https://doi.org/10.1016/j.compositesa.2016.06.018.

[9] G. Dean, L. Crocker, The use of finite element methods for design with adhesives, Measurement Good Practice Guide 48 (Mar. 2023), https://doi.org/10.47120/npl.mgpg48.

[10] X.P. Morelle, J. Chevalier, C. Bailly, T. Pardoen, F. Lani, Mechanical characterization and modeling of the deformation and failure of the highly crosslinked RTM6 epoxy resin, Mech. Time-Dependent Mater. 21 (3) (Aug. 2017) 419–454, https://doi.org/10.1007/s11043-016-9336-6.

[11] D. Thomson, et al., Numerical prediction of the ballistic performance of hygrothermally aged CFRP laminates using a multi-scale modelling approach, EPJ Web Conf. 250 (Sep. 2021), 03008, https://doi.org/10.1051/epjconf/202125003008.

[12] M. Herráez, A.C. Bergan, C.S. Lopes, C. González, Computational micromechanics model for the analysis of fiber kinking in unidirectional fiber-reinforced polymers, Mech. Mater. 142 (Mar. 2020), 103299, https://doi.org/10.1016/j.mechmat.2019.103299.

[13] L. Wan, et al., Computational micromechanics-based prediction of the failure of unidirectional composite lamina subjected to transverse and in-plane shear stress states, J. Compos. Mater. (Apr. 2020), 002199832091801, https://doi.org/10.1177/0021998320918015.

[14] J.K. Banerjee, Barreling of solid cylinders under axial compression, J. Eng. Mater. Technol. 107 (2) (Apr. 1985) 138–144, https://doi.org/10.1115/1.3225789.

[15] M. Jerabek, Z. Major, R.W. Lang, Uniaxial compression testing of polymeric materials, Polym. Test. 29 (3) (May 2010) 302–309, https://doi.org/10.1016/j.polymertesting.2009.12.003.

[16] B. Pan, Z. Lu, H. Xie, Mean intensity gradient: an effective global parameter for quality assessment of the speckle patterns used in digital image correlation, Opt Laser. Eng. 48 (4) (Apr. 2010) 469–477, https://doi.org/10.1016/j.optlaseng.2009.08.010.

[17] G. Quino, et al., Speckle patterns for DIC in challenging scenarios: rapid application and impact endurance, Meas. Sci. Technol. 32 (1) (Jan. 2021), 015203, https://doi.org/10.1088/1361-6501/abaae8.

[18] F. Lani, X. Morelle, C. Bailly, T. Pardoen, Characterization and modeling of the strain-rate, temperature and pressure dependence of the deformation of a highly crosslinked aerospace grade epoxy resin, in: ICCM International Conferences on Composite Materials, Copenhagen, 2015.

[19] M.C. Boyce, E.M. Arruda, An experimental and analytical investigation of the large strain compressive and tensile response of glassy polymers, Polym. Eng. Sci. 30 (20) (Oct. 1990) 1288–1298, https://doi.org/10.1002/pen.760302005.

[20] R.N. Haward, G. Thackray, The use of a mathematical model to describe isothermal stress-strain curves in glassy thermoplastics, Proc. R. Soc. A 302 (1471) (Jan. 1968) 453–472, https://doi.org/10.1098/rspa.1968.0029.

[21] E.M. Arruda, M.C. Boyce, Evolution of plastic anisotropy in amorphous polymers during finite straining, Int. J. Plast. 9 (6) (Jan. 1993) 697–720, https://doi.org/10.1016/0749-6419(93)90034-N.

[22] A.S. Argon, A theory for the low-temperature plastic deformation of glassy polymers, Phil. Mag. 28 (4) (Oct. 1973) 839–865, https://doi.org/10.1080/14786437308220987.

[23] G. Quino, A. Pellegrino, V.L. Tagarielli, N. Petrinic, Measurements of the effects of pure and salt water absorption on the rate-dependent response of an epoxy matrix, Compos. B Eng. 146 (Aug. 2018) 213–221, https://doi.org/10.1016/j.compositesb.2018.03.044.

[24] S. Pandini, A. Pegoretti, Time, temperature, and strain effects on viscoelastic Poisson's ratio of epoxy resins, Polym. Eng. Sci. 48 (7) (Jul. 2008) 1434–1441, https://doi.org/10.1002/pen.21060.

[25] M. Rueda-Ruiz, B.D. Beake, J.M. Molina-Aldareguia, Determination of rate-dependent properties in cohesive frictional materials by instrumented indentation, J. Occup. Med. 74 (6) (Jun. 2022) 2206–2219, https://doi.org/10.1007/s11837-022-05268-2.

[26] L. Wan, et al., Computational micromechanics-based prediction of the failure of unidirectional composite lamina subjected to transverse and in-plane shear stress states, J. Compos. Mater. (Apr. 2020), 002199832091801, https://doi.org/10.1177/0021998320918015.

[27] C. Sorini, A. Chattopadhyay, R.K. Goldberg, An improved plastically dilatant unified viscoplastic constitutive formulation for multiscale analysis of polymer matrix composites under high strain rate loading, Compos. B Eng. 184 (Mar. 2020), 107669, https://doi.org/10.1016/j.compositesb.2019.107669.

[28] A. Shundo, S. Yamamoto, K. Tanaka, Network Formation and physical properties of epoxy resins for future practical applications, JACS Au 2 (7) (Jul. 2022) 1522–1542, https://doi.org/10.1021/jacsau.2c00120.

[29] A. Shundo, M. Aoki, S. Yamamoto, K. Tanaka, Cross-linking effect on segmental dynamics of well-defined epoxy resins, Macromolecules 54 (13) (Jul. 2021) 5950–5956, https://doi.org/10.1021/acs.macromol.1c00513.

[30] J.J. Max, C. Chapados, Infrared spectroscopy of acetone–water liquid mixtures. I. Factor analysis, J. Chem. Phys. 119 (11) (Sep. 2003) 5632–5643, https://doi.org/10.1063/1.1600438.

[31] Q. Peng, B. Deng, M. Utz, Reduced plastic dilatancy in polymer glasses, Macromol. Theory Simul. 30 (2) (Mar. 2021), 2000063, https://doi.org/10.1002/mats.202000063.